PHYSICAL REVIEW B VOLUME 25, NUMBER 3 1 FEBRUARY 1982

Electronic structure and superconductivity in metal hexaborides

G. Schell, H. Winter, H. Rietschel, and F. Gompf
Kernforschungszentrum Karlsruhe, 7500 Karlsruhe, Postfach 3640, Federal Republic of Germany
(Received 28 July 1981)

The electronic structure and the phonon modes of the superconducting cluster compounds LaB_6 and YB_6 are evaluated. They are used to calculate the Eliashberg function of both compounds within the rigid-muffin-tin approximation for electron-phonon coupling. The individual contributions from the different phonon branches are discussed. It turns out that nonlocal corrections to the electron-phonon coupling are essential for those modes where the B_6 octahedras move as a whole. Omission of these corrections leads to a large overestimate of λ and T_c.

I. INTRODUCTION

Metal hexaborides of chemical composition MB_6 crystallize in the cubic structure. M may be an alkaline, earth alkaline- , lanthanide- , or actinide-group atom. In addition, the compound YB_6 exists. Hexaborides belong to the class of the cluster compounds because the boron atoms are grouped into octahedra. Both the metal atoms and the boron octahedra form simple cubic sublattices. In the cubic unit cell, a metal atom is sitting at the center and the centers of the boron octahedra are at its corners (Fig. 1 shows this structure). Many properties of the hexabordies seem to be due to the boron sublattice. The metal atoms, however, are necessary to stabilize the structure. This is similar to the situation in the molybdenum chalcogenide-Chevrel phases where the molybdenum atoms are the counterpart of the boron atoms in the compounds considered here.

Hexaborides possess a number of characteristics associated with good superconductors: they have nine branches of low-frequency phonon modes and a relatively high density of scattering centers in the form of boron atoms. With these properites one might expect a high T_c as is found for the PdH system. In that compound, the hydrogen atoms are strong *s-p* scatterers and the coupling of the electrons to the hydrogen vibrations is mainly responsible for its high transition temperature.[1]

In a local theory where we just add up the scattering intensities of the sites belonging to a unit cell, the volume density of atoms is of great importance. Its value for the hexaborides of about 1 atom per 9.9 Å^3 is not much below that of PdH where it amounts to 1 atom per 8.25 Å^3. Of course these considerations are only valid if the boron atoms have good single-site scattering properties. H in PdH has been found to be a strong *s-p* scatterer near the Fermi energy,[1] and for the boron atoms in the hexaborides, on the other hand, we expect good *p-d* scattering. If this is the case, the dominant contribution to the McMillan parameter λ[2] should come from the boron sublattice due to the high density of the boron atoms. However, experiment seems to tell a different story. To our knowledge there are only two superconducting metal hexaborides: LaB_6 and YB_6, with moderate transition temperatures (0.45 K for LaB_6 and 7.1 K for YB_6). A further surprise is the large difference in the T_c's of these two compounds since their lattice constants are almost the same (4.154 Å for LaB_6 and 4.113 Å for YB_6), and therefore their boron sublattices are nearly identical. The lattice

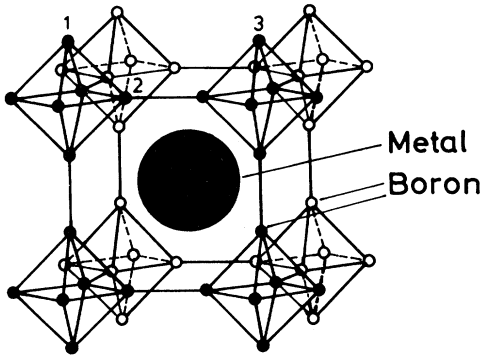

FIG. 1. Structure of hexaborides. The numbers indicate the atoms chosen as partners for a Keating-type angular-force constant in our phonon model.

constants of the nonsuperconducting hexaborides differ from that of LaB_6 by at most 4%. In the subsequent sections, we shall clarify this situation.

Analogies to the Chevrel phases exist in view of the superconducting properties. The molybdenum atoms there have been shown to be strong *d-f* scatterers. Their *d*-wave parts of the wave functions are well located within the octahedra.[3,4] The nature of their low-frequency phonon modes is very similar to that of the hexaborides where they consist of torsional and translational motions of the octahedra involving no deformations at the Γ point. So, a study of the electron coupling to these modes in the hexaborides should give us some insight into the mechanisms working also in the Chevrel phases.

This paper is organized as follows. Section II describes the detailed electronic structure calculations with special stress on the results significant for superconductivity. In Sec. III we analyze the characteristics of the different phonon modes and develop a simple phonon model fitted and compared to experiment. The results of Secs. II and III are used to calculate the Eliashberg function, the mass enhancement, and the transition temperature of LaB_6 and YB_6, in Sec. IV. We conclude with a discussion which answers the questions of the Introduction in light of our computational results.

II. THE ELECTRONIC STRUCTURE

The electronic structure has been calculated with the fast-symmetrized-cluster approach described in Ref. 5. For exchange and correlation, we use the Hedin-Lundqvist formula.[6] Self-consistency has been obtained after about 20 iterations in a system consisting of five shells of atoms with a boron octahedron in the center. The clusters used in these computations contained complete octahedra only. In a muffin-tin construction of the potential the values 0.5 and 0.2 have been chosen for the muffin-tin spheres of the metal and boron atoms, respectively, filling 73% of the space. Both the spheres of neighboring boron and metal atoms touch. From our look at a pointwise construction of the potential, we expect the asphericities within and the spatial variations outside the muffin-tin regions not to influence the results for the electronic structure essentially. The self-consistent potentials have been used to obtain the one-particle Green's functions employed in the succeeding calculations for clusters with 11 shells of atoms. The total densities of states (DOS) for LaB_6 and YB_6 resulting from these calculations are given in Fig. 2.

The features of the DOS are quite similar for both compounds. The only differences are the semicore *p* states of the lanthanum atom leading to the peak near -0.3 Ry which is not split because our calculations are nonrelativistic. The peak at -0.05 Ry in LaB_6 (0.01 Ry in YB_6) corresponds to states of A_{1g} symmetry with intraoctahedron binding character. Ascending the energy scale further, we find T_{1u} states between 0.15(0.2) and 0.40(0.45) Ry, A'_{1g}, T'_{1u}, and E'_g states in the range between 0.26(0.3) and 0.58(0.68) Ry, and T_{2g} states between 0.48(0.5) and 0.84(0.9) Ry. T_{2u} states are found for energies above ~ 0.95 Ry. T_{2g} and T_{2u} states are energetically separated, which leads to the range of low DOS with the minimum at 0.85(0.9) Ry.

For both compounds, the Fermi energy falls into the steeply ascending part of the DOS curve above the minimum. Summarizing, we can say that the sequence of the octahedron states found in our calculations is in accordance with the tight-binding results of Ref. 7 where only the boron sublattice is considered, while the influence of the metal atom

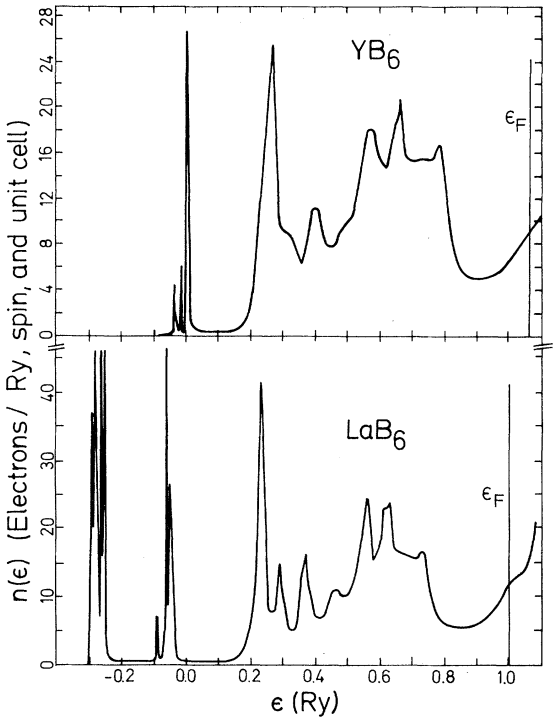

FIG. 2. Total electronic density of states for LaB_6 and YB_6.

is neglected. The states with significant contributions to the DOS from metal-atom regions lie above ~ 0.85 Ry. They are mainly of d character but near the Fermi energy there is considerable admixture of f states to the DOS. For LaB_6 the f contribution leads to a peak in the DOS at 1.14 Ry. These f states, however, are not well localized near the metal atoms. Instead, their radial functions are large in the outer regions of the metal muffin-tin spheres. It is important to remark that g contributions from the metal regions turned out to be quite negligible.

Our present results represent an improvement of preliminary calculations published in Ref. 8. In this earlier work, the metal muffin-tin radii have been fixed at the much smaller value of 0.35. Owing to the smaller metal muffin-tin radii the variations of the potentials outside the muffin-tin spheres have been larger in those former calculations than in the present ones.

The comparison of our results to the augmented-plane-wave (APW) band-structure work for LaB_6 of Ref. 9, where similar values for the muffin-tin radii been used, shows general agreement. The non-self-consistent band-structure calculations of Ref. 10, which go beyond the muffin-tin approximation, differ in important respects from both the APW results and our findings. The narrow A_{1g} peak, for example, is missing there and the total DOS value at ϵ_F (3.35 states per Ry spin unit cell) is below the value compatible with experiment. In the case of YB_6 no self-consistent band-structure calculations are known to us.

Comparing our results to experiment, we can state the following: they are compatible with the x-ray-photoemission-spectroscopy (XPS) measurements for LaB_6 (Refs. 11 and 12) and YB_6.[13] The evaluation of transition probabilities for bremsstrahlung processes with the use of our cluster data leads to good agreement with the experimental results.[14] Extraction of the DOS at the Fermi energy from specific-heat experiments is difficult because the numbers given in literature scatter by almost a factor of 2. In addition, due to the presence of low-frequency phonon modes, the separation between phononic and electronic contributions leads to further uncertainties. To our knowledge there are three experiments for LaB_6.[15–17] If we take the value extracted in Ref. 15 from experiments and correct for the mass-enhancement factor with our calculated λ value of 0.33, we end up with 10.28 states per Ry spin unit cell for the bare DOS compared to a value of 10.97 obtained with our cluster approach (the other authors get lower values). A similar analysis of the experimental data for YB_6 (Ref. 17) corrected with our $\lambda = 0.48$ leads to 5.5 states per Ry spin unit cell, while our calculated number is 8.87.

We used our calculated phonon spectra to estimate the error made by assuming a T^3 law when separating off the phonon contributions and came to the conclusion that this may lead to an underestimation of the DOS value of more than 50% in both substances.

The values of the electronic quantities needed for an evaluation of the Eliashberg function in the Gaspari-Gyorffy approximation are given in Table I. The numbers for YB_6 and LaB_6 are comparable. The scattering power[11] of YB_6 is slightly higher than that of LaB_6. For both metal and boron atoms, p-d scattering dominates. Of course, the small values of $\sin\delta_2$ for the metal atoms are caused by the fact that the phase shifts are evaluated at the boundaries of large muffin-tin spheres, and one could argue whether it is reasonable to use the rigid-muffin-tin approximation for the

TABLE I. Phase shifts δ_l, partial-density-of-states ratios $n_l/n_l^{(0)}$, and scattering powers η for LaB_6 and YB_6; these quantities are needed in order to calculate the Eliashberg function in the local approximation.

		δ_0	δ_1	δ_2	δ_3	$n_0/n_0^{(0)}$	$n_1/n_1^{(0)}$	$n_2/n_2^{(0)}$	$n_3/n_3^{(0)}$	η(eV/Å)^2
LaB_6	La	0.92	−1.39	0.078	−0.024	0.11	0.35	0.36	1.06	0.255
$\epsilon_F = 1.003$ Ry										
$n(\epsilon_F) = 10.86$										
(states per Ry spin unit cell)	B	−2.70	0.89	0.02		0.17	0.40	1.38		0.594
YB_6	Y	−2.02	1.89	3.15	−0.17	0.17	0.28	0.42	1.19	0.328
$\epsilon_F = 1.061$ Ry										
$n(\epsilon_F) = 8.87$										
(states per Ry spin unit cell)	B	−2.77	0.85	0.02		0.23	0.41	1.29		0.709

electron-phonon coupling matrix elements at these sites. However, the main contributions to the Eliashberg functions $\alpha^2F(\omega)$ come from the boron sites, and this uncertainty is not so important in connection with the problems we are mainly treating in this paper. As we shall discuss in Sec. IV, it is essential to go beyond the local Gaspari-Gyorffy[18] approximation. Therefore, in addition, we need matrix elements of the imaginary part of the scattering path operator at the Fermi-energy nondiagonal in both the sites and the angular momentum variables. Our use of scattering theory provides us with all of these quantities in a direct manner.

In order to work with the least possible number of data, the matrix elements which we use are those between the shell-symmetrized states defined in Ref. 5. Single-site angular-momentum eigenstates for atoms belonging to the same sort and having equal distances from the point center of the cluster are linearly combined to form basis states of the irreducible representations of the crystal-point group. The quantum numbers $|M\nu s\kappa\rangle$ identifying these states have the following meanings: M is the label of the irreducible representation, ν is the label of the basis state, s is the label of the atoms contributing to $|M\nu s\kappa\rangle$, and κ is the label of a state with the aforementioned quantum numbers.

The single-site states combined to a symmetrized state $|M\nu s\kappa\rangle$ all belong to the same angular momentum. Because the scattering matrix elements are diagonal in quantum numbers ν,ν' and independent of ν, we write them in the following manner:

$$\tilde{T}^{M}_{s\kappa,s'\kappa'}(\epsilon_F)=-\frac{\mathrm{Im}T^{M}_{s\kappa,s'\kappa'}(\epsilon_f)\sqrt{\epsilon_F}}{(\sin\delta_{l'(M,s',\kappa')}\sin\delta_{l'(M,s',\kappa')})} \ . \tag{1}$$

For an atom at the symmetry-group-point center, the elements of $\tilde{T}$ diagonal in the s,κ indices are just the ratios of the local DOS intoduced in Ref. 18. The matrix elements of $\tilde{T}$ with respect to the symmetrized states derived from single-site p and d states at the boron atoms of one octahedron are displayed in Table II for YB_6. We see that the matrix elements of states belonging to the T_{2u} representation ($M=6$) predominate. This is in accordance with the features of the DOS near the Fermi energy. Their contribution to the space-dependent DOS at ϵ_F, given by the relation

$$n(\vec{r};\epsilon_F)=-\frac{2}{\pi}\mathrm{Img}(\vec{r},\vec{r};\epsilon_F) \ , \tag{2}$$

is shown in Fig. 3. Here Img is the imaginary part of the one-particle Green's function. It is large in the range of the boron octahedra. However, a binding DOS between neighboring octahedra also exists.

III. THE PHONON MODES

The cluster structure of the hexaborides leads to very different vibrational characteristics for the 21 phonon branches. We obtained their classification by constructing the symmetry-adapted polarization vectors at the Γ point. The 0_h-group projection operators have been applied to the Cartesian components of the displacement vectors for this purpose. This procedure is analogous to that employed in the symmetrized version of the electronic structure calculations. The result of this analysis is displayed in Fig. 4. The polarization vectors are given together with the symbols for the irreducible representation to which the corresponding modes belong. Considering the boron atoms, the Γ-point vibrations may be separated into two classes: the first is associated with deformations of the octahedra, while in the second the octahedra move undeformed. It is the latter one which is expected to contain the low-frequency vibrations: the threefold-degenerate torsional mode (T_{1g}) and two threefold-degenerate translational (T_{1u}) modes.

The T_{1u} modes of the boron sublattice may be combined with the T_{1u} modes of the metal sublattice to lead to three acoustic branches on the one hand, and to three optical branches on the other. Provided the coupling to the electrons is sufficiently strong, these modes should be particularly important for superconductivity due to their low frequencies. The deformation modes should occur at substantially higher frequencies on account of the strong binding between the atoms of one octahedron. The breathing mode (A_{1g}) and E_g mode connected with particularly large changes of intraoctahedron-bonding lengths and angles should lie at the top of the frequency scale. That is all we can say from looking at the structure. For a detailed positioning of the peaks in the phonon DOS and the calculation of the dispersion of the different branches, we have to resort to a phonon model using parameters fitted to experiment. The experimental information is rather incomplete however. For LaB_6, it is better than for YB_6.

TABLE II. Values of some matrix elements $\tilde{T}^{M}_{s\kappa,s'\kappa'}$ for the boron octahedron; 1, 1′ are the angular momenta associated with the states $|M\kappa s\rangle$, $|M\kappa' s'\rangle$.

	$M=1$		2			3				4			
κ',s',l' / κ,s,l	3,1,2	5,1,1	3,1,2		3,1,2	4,1,2	7,1,1		3,1,2	5,1,1	6,1,1	9,1,2	
3,1,2	0.345	0.105	3,1,2	0.044	3,1,2	0.303	0.439	0.111	3,1,2	0.061	0.048	0.0003	0.004
5,1,1	0.105	0.047			4,1,2	0.439	0.666	0.203	5,1,1	0.048	0.147	0.065	0.541
					7,1,1	0.111	0.203	0.085	6,1,1	0.0003	0.065	0.032	0.245
									9,1,2	0.004	0.541	0.245	3.33

	$M=5$			6				7			8		9	
κ',s',l' / κ,s,l	2,1,1	4,1,2	5,1,2		1,1,2	3,1,1	5,1,2		1,1,1	3,1,2		1,1,2		2,1,2
2,1,1	0.343	0.571	0.349	1,1,2	4.84	2.97	2.73	1,1,1	0.094	0.266	1,1,2	0.006	2,1,1	0.008
4,1,2	0.571	0.969	0.576	3,1,1	2.97	1.78	1.74	3,1,2	0.266	0.757				
5,1,2	0.349	0.576	0.364	5,1,2	2.73	1.74	1.74							

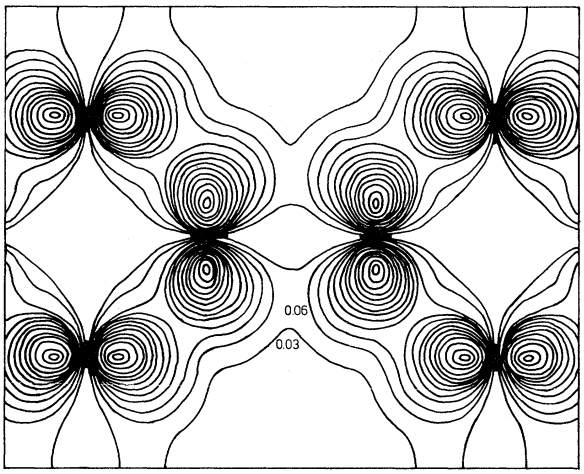

FIG. 3. Spatial density of states distribution at the Fermi energy around the boron atoms for YB_6. The units are: states per [spin Ry (a.u.)^3]. The symbols | indicate the position of the boron atoms. The increment between two adjacent lines is 0.03.

Raman-scattering experiments[19–21] give the frequencies of the A_{1g}, E_g, and T_{2g} modes at the Γ point for LaB_6. In the case of YB_6 only the frequency of the T_{1g} mode is known from this type of experiment.[20,22]

One of us (FG) performed inelastic-neutron-scattering experiments on polycrystalline LaB_6 and YB_6 in the energy-loss mode using an incoming energy E_0 of 64.3 meV at the research reactor FR2 of the Kernforschungszentrum Karlsruhe. The results for the lowest-frequency mode as registered in the time-of-flight channels are shown in Fig. 5. The background has been substracted. The position of the peak corresponds to 13 meV in the case of LaB_6 and 10 meV in the case of YB_6. Due to intensity problems connected with the high-neutron-absorption cross section of the ^{10}B atoms, no other modes could be measured in this first at-

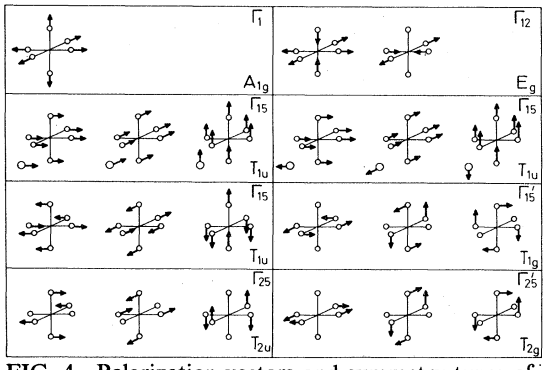

FIG. 4. Polarization vectors and symmetry types of the phonons at the Γ point.

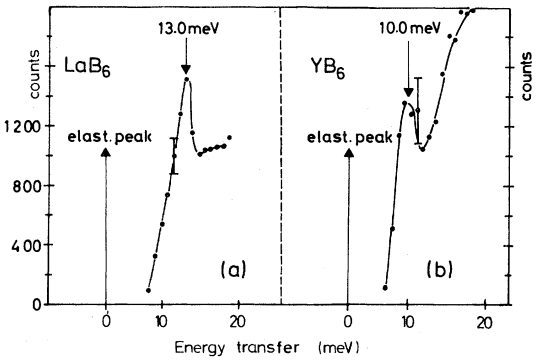

FIG. 5. Time-of-flight spectra of neutron scattering experiments in the energy range of the lowest phonon DOS peaks.

tempt. Further experiments were then carried out with $E_0 = 5$ meV (FR2 — Karlsruhe) and with $E_0 = 4.88$ meV (HFR — Grenoble) for LaB_6 and CeB_6 using ^{11}B-enriched boron compounds. A comparison between the scattering intensities of the lowest modes in LaB_6 and CeB_6, which appear for the same energy transfer since La and Ce have practically equal atomic masses, leads us to the conclusion that the lowest frequency peak is due to the acoustic translational T_{1u} and not to the torsional T_{1g} mode, because the difference in the scattering intensities can only be understood if one takes into account that the scattering cross section of Ce is much smaller than that of La (a detailed description of these results will be given in Ref. 23). From these experiments we conclude that electronic effects push the frequencies of the translational modes in YB_6 below those of LaB_6 in spite of the fact that the Y atom has a smaller mass than La.

In view of the limited experimental information only a simple phonon model is justified (central forces between nearest-neighbor and next-nearest-neighbor boron atoms together with a metal nearest-neighbor boron-atom central force). In the case of LaB_6, a fit of these involved three parameters to the highest Raman frequencies and the acoustic translational-mode peak was unable to place the torsional mode at the right position. The introduction of further central forces also failed to achieve this and to simultaneously maintain the weak dispersion of the torsional mode. Instead, it proved necessary to introduce a Keating force[24] into the model derived from a potential which depends on the position of three atoms. By far, the best fit to experiment has been achieved by choosing the boron atoms with the labels 1,2,3 in

Fig. 1 as partners for these interactions. Figure 6 shows the resulting phonon DOS for LaB_6 together with the generalized DOS obtained from the data of the aforementioned experiment. We find satisfying agreement between experiment and theory. The four characteristic vibrations involving the underformed octahedron, i.e, (i) the translation mode B_6-La at 13 meV, (ii) the rotation mode B_6-B_6 at about 38 meV, and (iii) the optical modes B_6-La at 24 meV and around 55 meV are all nicely found in the measured spectrum.

Octahedron deformation modes which for the experimental curve are smeared out due to lack of resolution, have been found between 60 and 120 meV. At higher frequencies the experiment runs out of intensity. The calculated frequencies in this range are about 8% too low. Figure 7 shows the phonon dispersion along some symmetry directions in the Brillouin zone. The results encouraged us to apply this model also to YB_6. For this compound, no experimental information on Raman scattering was available. So, we extrapolated the data for other trivalent transition metals as a function of lattice constant to the case of YB_6. Together with the frequency of the acoustic translational mode the experimental information was then sufficient to fit the parameters of our phonon model. The phonon DOS curve of YB_6 is shown in Fig. 9(a). The frequency of the torsional mode for YB_6 is now predicted to lie at 30 meV. The nondeformation modes of YB_6 are all below those of LaB_6, a finding which is important if we compare the superconducting properties of both substances to each other.

IV. THE ELIASHBERG FUNCTION

The results of the preceding chapters enable us to calculate the Eliashberg functions $\alpha^2F(\omega)$ treating electron-phonon coupling in the rigid-muffin-tin approximation (called RMTA hereafter). It may be written in the following way:

$$\alpha^2F(\omega)=\sum_{j,j'}[\alpha^2F(\omega)]_{j,j'}=\frac{1}{2\pi^2 n(\epsilon_F)}\sum_{j,j',\lambda}\int d\vec{q}\,d\vec{\rho}\,d\vec{\rho}''\delta(\omega-\omega_{\vec{q},\lambda})/[\omega(M_jM_{j'})^{1/2}\rho\rho']$$
$$\times\mathrm{Re}\{\exp[i\vec{q}(\vec{R}_j-\vec{R}_{j'})](\vec{e}^{\,j}_{\vec{q},\lambda}\cdot\vec{\rho})(\vec{e}^{\,j'*}_{\vec{q},\lambda}\cdot\vec{\rho}')\}$$
$$\times\frac{dV^j(\rho)}{d\rho}\frac{dV^{j'}(\rho')}{d\rho'}[\mathrm{Img}(\vec{\rho}j,\vec{\rho}'j';\epsilon_F)]^2\,. \tag{3}$$

Here, g is the retarded Green's function, V^j is the muffin-tin potential of site j, and the coordinate $\vec{\rho}$ ($\vec{\rho}''$) is counted from site j (j') at position $\vec{R}_j$ ($\vec{R}_{j'}$). $\omega_{\vec{q},\lambda}$ is the frequency and $\vec{e}_{\vec{q},\lambda}$ the amplitude of a phonon with wave vector $\vec{q}$ belonging to the branch λ. The sum over j is restricted to the atoms of one unit cell, whereas the sum over j' is unrestricted.

Omitting all terms with $j\neq j'$ we obtain $\alpha^2F(\omega)$ in the local rigid-muffin-tin approximation[18] (LRMTA). As we shall see below, neglecting those off-diagonal terms is a rather poor approximation in the case of the cluster compounds we are considering in this paper. Instead, it proved essential to work with the full Eq. (3). We found it convenient to express the Green's function occurring in Eq. (3) by the matrix elements of the scattering path operator between the shell-symmetrized states as described in Sec. II. The electronic contributions of Eq. (3) may then be separated into a part which depends on the crystal structure on the one hand and the matrix elements on the other. We obtain

$$\alpha^2F(\omega)=\frac{1}{2\pi^2 n(\epsilon_F)}\sum_{s,s'}\sum_{\substack{M\\ \kappa,\kappa'}}\sum_{\substack{M_1\\ \kappa_1,\kappa_1'}}\sum_{\lambda}\int d\vec{q}\,\frac{\delta(\omega-\omega_{\vec{q},\lambda})}{(M_sM_{s'})^{1/2}\omega}B^{M\ M_1}_{s\kappa\kappa_1;\,s'\kappa'\kappa_1'}(\vec{q},\lambda)\tilde{T}^{M}_{s\kappa,s'\kappa'}(\epsilon_F)\tilde{T}^{M_1}_{s\kappa_1,s'\kappa_1'}(\epsilon_F)$$
$$\times[\sin(\delta^{(s)}_{l_1(M_1s\kappa_1)}-\delta^{(s)}_{l(Ms\kappa)})\Delta_{l,l_1+1}+\sin(\delta^{(s)}_{l}-\delta^{(s)}_{l_1})\Delta_{l_1,l+1}]$$
$$\times[\sin(\delta^{(s')}_{l'(Ms'\kappa')}-\delta^{(s)}_{l_1',(M_1,s',\kappa_1')})\Delta_{l_1',l'+1}+\sin(\delta^{(s')}_{l_1'}-\delta^{(s')}_{l'})\Delta_{l',l_1'+1}]\,, \tag{4}$$

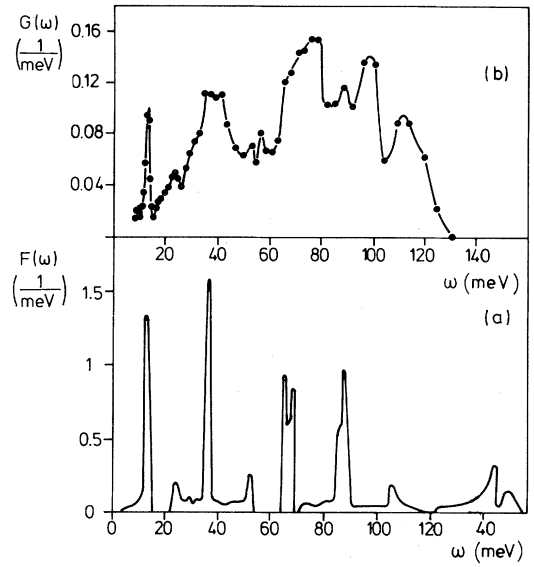

FIG. 6. Comparison between the measured (b) and calculated (a) phonon DOS of LaB_6.

s,s' are the shell indices. The meaning of the labels occurring in Eq. (4) has been explained in Sec. II. The quantity B contains the structural electronic quantities described in Ref. 5 together with the phonon-polarization vectors. According to Secs. II and III for $\vec{q}\to 0$, B is determined by symmetry alone.

Comparing the values for the elements of B obtained by an exact calculation with those of the local approximation (la) in Table IV we see large differences. Some of these elements are even zero in the la. If the corresponding $\tilde{T}^M$ happens to be large, the local approach fails. We calculated $\alpha^2F(\omega)$ for the different modes separately. The results for LaB_6 are shown in Fig. 8 and for YB_6 in Fig. 9 for both the full calculation and within la. The function $\alpha^2(\omega)$ in Figs. 8 and 9 is defined as the ratio of $\alpha^2F(\omega)$ and $F(\omega)$ may be interpreted as the $\vec{q}$- and branch-averaged electron-phonon coupling at ω. For both compounds the curves are looking quite similar. The most striking feature is that the nonlocal effects lead to a strong depression of the electron coupling to the nondeformational low-frequency modes over their whole energy range. The overall coupling to the deformation modes is similar to the local result with the exception of the T_{1g} mode. The coupling to this mode is largely enhanced as compared to the local result. Due to the high frequency of this mode, however, it is only of minor importance for superconductivity. The contributions to the McMillan parameters λ are listed in Table III. The numbers for the total λ's again stress the necessity for a calculation to go beyond the la.

It is instructive to trace back the origin of the large nonlocal corrections. Our calculations have shown that the main nonlocal contributions come from the atoms of the same octahedron. As already stated in Sec. II, the matrix elements of $\tilde{T}$ belonging to the $T_{2u}(M=6)$ representation and

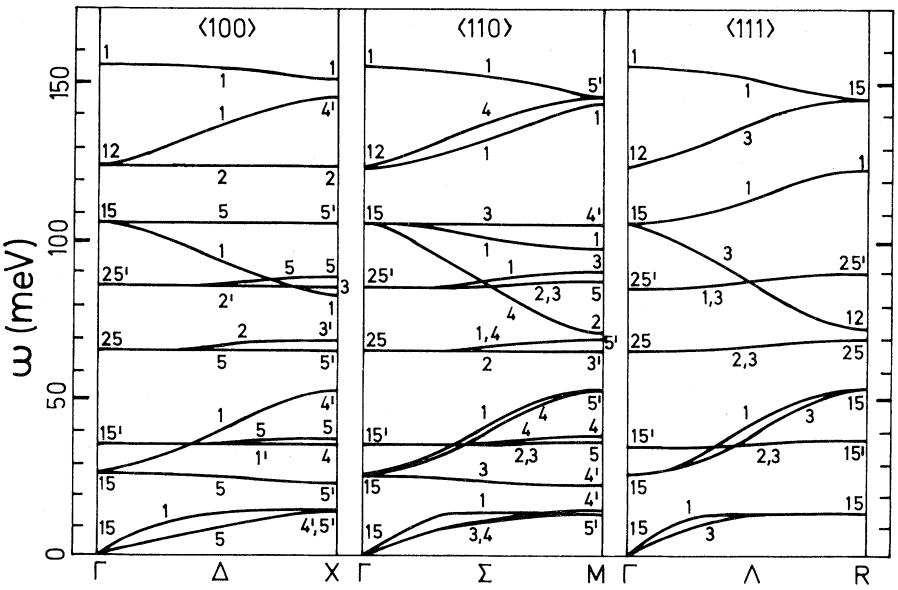

FIG. 7. Phonon dispersion for LaB_6 along selected symmetry directions as obtained by our model.

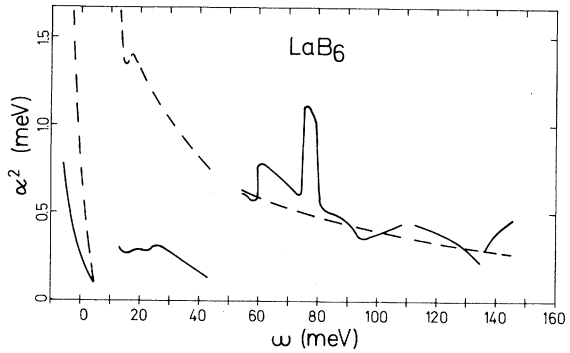

FIG. 8. Frequency-dependent coupling function $\alpha^2(\omega)$ for LaB_6; solid line, nonlocal calculation; dashed line, local approximation.

leading to the charge distribution shown in Fig. 3 dominate. In Table IV we list the elements of B for these quantum numbers at $\vec{q}=0$. Combining them with the corresponding $\tilde{T}$-matrix elements of Table II and performing the sums of Eq. (3), we observe an almost perfect cancellation between the individual terms. The la misses this point because it puts some elements of B equal to zero. For the T_{2g} phonon mode the values of the B coefficients lead to constructive interference and therefore cause the large enhancement of α^2 over its value in la.

We calculated the transition temperatures of both compounds by solving the Eliashberg equation with our calculated $\alpha^2F(\omega)$ numerically. We found $T_c = 0.78$ K for LaB_6 and $T_c = 3.85$ K for YB_6. In la we got 9.81 K for LaB_6 and 23 K for YB_6, results which underline the necessity of nonlocal corrections.

V. SUMMARY AND DISCUSSION

We are now in a position to discuss the questions raised in Sec. I in the spirit of our calcula-

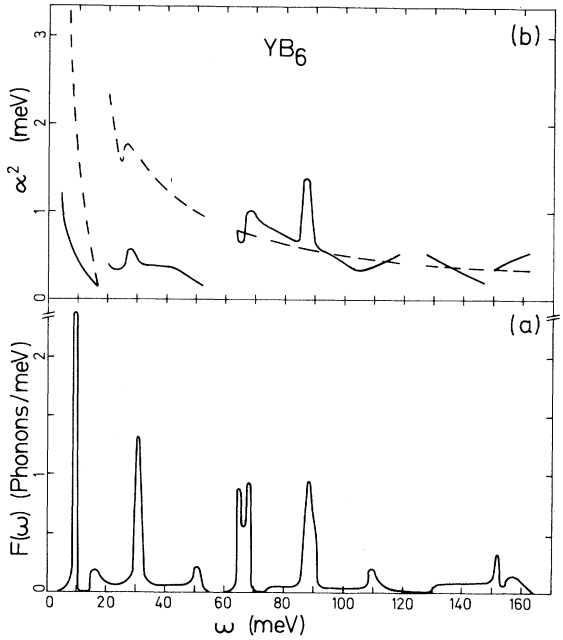

FIG. 9. (a) Phonon density of states for YB_6 as obtained by our model. (b) Frequency-dependent coupling function $\alpha^2(\omega)$ for YB_6; solid line, nonlocal calculation; dashed line, local approximation.

tions. The boron atoms turned out to be rather strong *p-d* scatterers and could therefore lead to good superconducting properties in view of their high density and of the low frequencies of some of their phonon modes. The detailed calculations of the last section, however, show that large nonlocal contributions are very effective in depressing the single-site scattering values and suppressing the transition temperatures. This is different from the behavior of noncluster compounds where the sign of nonlocal corrections turns out to be strongly mode- and $\vec{q}$-vector dependent. For transition me-

TABLE III. Contributions of the individual phonon modes to the McMillan parameter λ.

Mode	LaB_6 nonlocal	LaB_6 local	YB_6 nonlocal	YB_6 local
T_{1u} (translational)	0.065	0.145	0.094	0.236
T_{1u} (optical)	0.040	0.193	0.058	0.234
T_{1g} (rotational)	0.053	0.198	0.121	0.395
T_{2u}	0.053	0.054	0.059	0.069
T_{2g}	0.081	0.036	0.100	0.042
T_{1u}	0.027	0.025	0.034	0.032
E_g	0.009	0.010	0.010	0.011
A_{1g}	0.005	0.004	0.006	0.004
Total λ	0.33	0.66	0.48	1.02

TABLE IV. Nonzero matrix elements $B^{6\ 6}_{s\kappa\kappa_1;s'\kappa'\kappa'_1}$ for $\vec{q} = 0$; the nonlocal matrix elements for the translational mode vanish.

	Translational mode, local					
$s\kappa\kappa_1$	1 1 1	1 3 3	1 3 3	1 3 5	1 5 3	1 5 5
$s'\kappa'\kappa'_1$	1 3 3	1 1 1	1 5 5	1 5 3	1 3 5	1 3 3
B	0.0239	0.0239	0.0119	0.0119	0.0119	0.0119

	Rotational mode, local		Rotational mode, nonlocal			
$s\kappa\kappa_1$	1 1 1	1 3 3	1 1 1	1 1 3	1 3 1	1 3 3
$s'\kappa'\kappa'_1$	1 3 3	1 1 1	1 3 3	1 3 1	1 1 3	1 1 1
B	0.0239	0.0239	0.0477	−0.0477	−0.0477	0.0477

tals nonlocal effects lead also to a reduction of $\alpha^2(\omega)$ on the average, while for some metal hydrides and the refractory coupounds the nonlocal corrections have been found to be small.[26–29] In the cluster substances considered in the present work, they are extremely large and one should be aware of the posibility of a similar situation in other cluster substances too. From isotope-effect measurements, Culetto and Pobell[30] drew the conclusion that the coupling to the low-frequency modes is also small in the molybdenum chalcogenides.

Their reasoning is that the d state at the molybdenum octahedra which are mainly responsible for superconductivity, are well localized with little overlap to the neighboring octahedra. Undeformed motion of the octahedra should therefore not change the energy contribution due to these d states. As a consequence, the effective coupling to the nondeformational modes should be small. In our case, the overlap of the relevant states between neighboring boron octahedra turned out to be nonnegligible, and as suggested by the behavior of the quantities B, we consider the large reduction in the electron-phonon coupling as a symmetry effect. That is, one must consider the boron octahedra as a unit and interference effects within this cluster are important in determining the final electron-phonon coupling.

Let us now return to the hypothesis that the boron sublattice is mainly responsible for superconductivity. This hypothesis seemed to contradict the observation that the T_c's of YB_6 and LaB_6 are different in spite of their almost identical lattice constants. This objection can be discarded by our results. We found that the main contributions to the McMillan parameters do really come from the boron sublattice. Both compounds, however, turn out to be weak-coupling superconductors. Moderate differences in the λ values therefore lead to large differences in the T_c's. Table I and Figs. 8 and 9(b) show that the electron-phonon coupling is somewhat larger in YB_6 and in addition, as mentioned in Sec. III, the non-deformational modes of YB_6 are lower in accordance with the differences in the electron-phonon coupling. In view of the smallness of the λ's, we consider our T_c calculations which clearly exhibit that YB_6 is the better superconductor as reasonable. A slightly higher λ value would be sufficient to bring the T_c of YB_6 to the experimental value.

Analogies to the molybdenum chalcogenides can be pointed out in view of the comparable nature of their phonon modes and the cluster entities they share in common and which are mainly responsible for superconductivity. Of course, the d-f scattering of the molybdenum atoms in the Chevrel phases is more favorable for superconductivity than the p-d scattering of the boron atoms in the hexaborides. So, as a difference the Chevrel phases seem to be strong coupling superconductors.

However, similar to the hexaborides, they show a strong reduction of the electron coupling to the nondeformational phonon modes by nonlocal scattering contributions. From our analysis it has become clear that T_c calculations based on approximate formulas like the McMillan formula and on only a few data like the total DOS at ϵ_F and the Debye frequency must fail. In such a crude approach it is especially unclear which frequency average has to be inserted as a prefactor of the exponential in the McMillan formula. In fact, considerations of this kind led to exaggerated expectations concerning the transition temperatures of the hexaborides.[10] Finally, we should like to remark that it would be highly desirable to obtain experimental information about the Eliashberg function from tunneling measurements.

[1]D. A. Papaconstantopoulos and B. M. Klein, Phys. Rev. Lett. 35, 110 (1975).
[2]W. L. McMillan, Phys. Rev. 167, 331 (1968).
[3]O. K. Andersen, W. Klose, and H. Nohl, Phys. Rev. B 17, 1209 (1978).
[4]T. Jarlborg and A. J. Freeman, *Superconductivity in d and f Band Metals* (Academic, New York, 1980), p. 521.
[5]G. Ries, and H. Winter, J. Phys. F 9, 1589 (1979).
[6]L. Hedin, and B. I. Lundqvist, J. Phys. C 4, 2064 (1971).
[7]H. C. Longuet-Higgins, and M. deV Roberts, Proc. R. Soc. London, A224, 336 (1954).
[8]G. Schell, H. Winter, and H. Rietschel, *Superconductivity in d and f Band Metals* (Academic, New York, 1980), p. 465.
[9]A. Hasegawa and A. Janase, J. Phys. F 7, 1245 (1977).
[10]P. F. Walch, D. E. Ellis, and F. M. Mueller, Phys. Rev. B 15, 18 (1977).
[11]J. N. Chazalviel, M. Campagna, G. K. Wertheim, and P. H. Schmidt, Solid State Commun. 19, 725 (1976).
[12]M. Aono, T. C. Chiang, J. A. Knapp, T. Tanaka, and D. E. Eastman, Phys Rev. B 21, 2661 (1980).
[13]M. Aono, S. Kawai, S. Kono, M. Okusawa, T. Sagawa, and Y. Takehana, J. Phys. Chem. Solids 37, 215 (1976).
[14]I. I. Lyakhovskaya, T. M. Zimkina, V. A. Fomichev, Fiz. Tverd. Tela (Leningrad) 12, 174 (1970) [Sov. Phys.—Solid State 12, 138 (1970)].
[15]J. Etournau, J. P. Mercurio, R. Naslin, and P. Hagenmuller, J. Solid State Chem. 2, 332 (1970).
[16]T. Kasuya, K. Takegahara, T. Eujita, T. Tanaka, and E. Bannai, J. Phys. (Paris) Colloq. 40, C 5—308 (1979).
[17]B. I. Matthias, T. H. Geballe, K. Andres, E. Corenzwit, G. W. Hull, and J. P. Maita, Science 159, 530 (1968).
[18]G. D. Gaspari and B. L. Gyorffy, Phys. Rev. Lett. 28, 801 (1972).
[19]H. Scholz, W. Bauhofer, and K. Ploog, Solid State Commun. 18, 1539 (1976).
[20]M. Jshii, M. Aono, S. Muranaka, and S. Kawai, Solid State Commun. 20, 437 (1976).
[21]M. Jshii, T. Tanaka, E. Bannai, and S. Kawai, J. Phys. Soc. Jpn. 41, 1075 (1976).
[22]G. Güntherodt, R. Merlin, A. Frey, and M. Cardona, Solid State Commun. 27, 551 (1978).
[23]F. Gompf, G. Löwenhaupt, and N. Nuecker, unpublished.
[24]P. N. Keating, Phys. Rev. 145, 637 (1966).
[25]G. Bergmann, and D. Rainer, Z. Phys. 263, 59 (1973).
[26]D. Glötzel, D. Rainer, and H. R. Schober, Z. Phys. B35, 317 (1979).
[27]H. Winter, and G. Ries, Z. Phys. B24, 279 (1976).
[28]H. Winter, H. Rietschel, G. Ries, and W. Reichardt, J. Phys. (Paris) 39, C 6—474 (1978).
[29]D. Glötzel, R. W. Simpson, and H. R. Schober, *Physics of Transition Metals, 1980,* edited by P. Rhodes (IOP, Bristol, 1980), p. 567.
[30]F. J. Culetto, and F. Pobell, Phys. Rev. Lett. 40, 16 (1978); 40, 1104 (1978).